Polymer 49 (2008) 3116–3124

Contents lists available at ScienceDirect

Polymer

journal homepage: www.elsevier.com/locate/polymer

Microphase separated structures in the solid and molten states of double-crystal graft copolymers of polyethylene and poly(ethylene oxide)

P.R. Mark [a], N.S. Murthy [a,b,*], S. Weigand [c], K. Breitenkamp [d], M. Kade [d], T. Emrick [d]

[a] Physics Department, University of Vermont, Burlington, VT 05405, United States
[b] New Jersey Center for Biomaterials, Rutgers University, Piscataway, NJ 08854, United States
[c] DND-CAT Synchrotron Research Center, Northwestern University, Advanced Photon Source, Argonne National Laboratory, Argonne, IL 60439, United States
[d] Department of Polymer Science and Engineering, University of Massachusetts Conte Center for Polymer Research, Amherst, MA 01003, United States

ARTICLE INFO

Article history:
Received 18 March 2008
Received in revised form 1 May 2008
Accepted 3 May 2008
Available online 15 May 2008

Keywords:
Microphase separation
Graft copolymers
Crystallization

ABSTRACT

Transitions from one microphase separated structure in the solid state to a different one in the molten state in polyethylene-*graft*-poly(ethylene oxide) copolymers, PE-*g*-PEO, were investigated by variable temperature X-ray scattering measurements and thermal analyses. Small-angle X-ray scattering patterns from polymers with PEO grafts with 25, 50 and 100 ethylene oxide (EO) units show that the polymer passes through three distinct structures at ~10 nm length scales with increase in temperature (T): lamellar structures of PE and PEO at $T < T_m^{PEO}$, PE lamellae surrounded by molten PEO at $T_m^{PEO} < T < T_m^{PE}$, and microphase separated structures at $T > T_m^{PE}$ when both PE and PEO are molten (T_m refers to the melting temperature). These phase transformations also occur during cooling but with hysteresis. Crystalline phases of PEO side chains and PE main chains could be identified in the wide-angle X-ray diffraction profiles indicating that the PE backbone and PEO grafts crystallize into separate domains, especially with longer grafted chains (50 and 100 units). At EO segment lengths > 50, PEO shows the expected increase in melting and crystallization temperatures with the increase in the grafted chain length. PE does not affect T_m^{PEO} but does decrease the onset of crystallization upon cooling. PEO grafts result in fractionation of PE, decrease the melting point of PE and increase the undercooling for the onset of crystallization of PE.

1. Introduction

Mixtures of homopolymers, even with only a slight difference in either the structure or the composition, invariably separate into macrophases. This tendency to phase separate on a macroscopic scale is frustrated when two incompatible chains are connected, in which case a complex array of nanophase and microphase separated structures occur. Control over polymer architecture to obtain desired microphase structures requires a fundamental understanding of such structures, both of which have implications on the use of these materials in biology and in more conventional use as engineering plastics. The large body of theoretical and experimental work on copolymers is described in frequently cited papers [1,2] and in several books [3–7]. Most of this literature is on diblock copolymers and investigations of microphase separation in copolymers with disordered sequences are less numerous. Much less is known about multi-block copolymers and graft copolymers. A study of random graft copolymers (RGCs), such as polybutadiene-*graft*-polystyrene, reported that microphase ordering occurs in melt [8]. Order–disorder transition has also been reported in RGCs with quenched sequence disorder in the solid state [9]. Here we discuss a graft copolymer in which both the components are crystallizable. The morphology in such systems depends on two self-organizing processes, crystallization and microphase separation [7].

RGCs with amphiphilic molecules have been shown to form micelles in slightly selective solvents [10]. Here we study the microphase separated structures in the solid state as well as in the melt of a branched amphiphile, polyethylene-*graft*-poly(ethylene oxide) (PE-*g*-PEO). PE-*g*-PEO is a double-crystal graft copolymer, and is expected to show a behavior that in some ways is different from other double-crystal block copolymers such as those made with PE and PEO [11], PE and poly(ε-caprolactone) (PCL) [12], PCL and poly(L-lactide) [13]. The PEGylated (PEG, poly(ethylene glycol), is an accepted synonym for PEO in the context of this paper) polyethylene structures make possible a systematic study of the influence of molecular level constraints on the structure and crystallization behavior of PE and PEO. These results are of practical significance because graft copolymers are widely used as compatibilizers of polymer blends, as well as surface modifiers and surfactants.

* Corresponding author. New Jersey Center of Biomaterials, Rutgers University, 145 Bevier Road, Piscataway, NJ 08854, United States. Tel.: +1 732 445 0488; fax: +1 732 445 5006.
E-mail address: murthy@biology.rutgers.edu (N.S. Murthy).

0032-3861/$ – see front matter © 2008 Elsevier Ltd. All rights reserved.
doi:10.1016/j.polymer.2008.05.012

2. Materials

The graft copolymers were prepared by ring-opening metathesis polymerization (ROMP) of cyclooctene and PEGylated cyclooctene using methods described previously [14]. Three samples were studied: PE-*g*-PEO**1**, PE-*g*-PEO**2** and PE-*g*-PEO**3**, containing approximately one PEO graft per 100 backbone carbons, about eight graft points per molecule on average, and graft lengths of 25, 50 and 100 repeat units, respectively. The details of the three copolymers are given in Table 1. PEO homopolymers (Clariant: PEG 2000 S Pharma; Fluka: PEG 5000) were also analyzed for comparison. The volume fractions shown were calculated assuming amorphous densities of PE and PEO to be 0.8246 and 1.0609 g/cm^3, respectively [15], and are given only for comparing the three copolymers.

3. Methods

Differential scanning calorimetry (DSC) was performed on TA Instruments' DSC 2010 with ~8 mg samples, and a heating rate of 10 °C per minute. The samples were melted, cooled and reheated.

Wide-angle X-ray diffraction (WAXD) scans at room temperature were obtained on a Rigaku Geigerflex and D/max-B diffractometer in the reflection geometry (wavelength $\lambda = 1.542$ Å, CuKα). These in-house X-ray diffraction (XRD) measurements were carried out on powdered samples spread into a thin layer on the sample holder. For variable temperature scans, a thin layer of thermal compound was spread on the copper heating block for good thermal contact as well as adhesion. Silicon powder was used as an internal standard. A Rigaku Rotaflex rotating anode with a Bruker GADDS 2D detector was used to obtain 2D XRD patterns from PE-*g*-PEO films.

Numerous X-ray scattering patterns were obtained in the 5ID-D enclosure of DND-CAT at the Advanced Photon Source ($\lambda = 1.0$ Å). Small-angle X-ray scattering (SAXS) patterns at ambient temperatures were obtained from powders in 1 mm quartz capillaries. Simultaneous SAXS–WAXD–DSC data were acquired in transmission mode through 6–9 mg of sample mounted in aluminum pans on a Linkam® CI93 DSC as the sample was heated at the rate of 10 °C/min. X-ray beam from a Si- (111) double-crystal monochromator was collimated with three sets of slits to about 0.2 mm × 0.2 mm. WAXD patterns were collected on a 100 mm × 200 mm dual chip Roper® CCD camera. Dark frame, distortion, and flat-field corrections were done with FIT2D [16]. SAXS patterns were simultaneously collected on a 165 mm diameter MarCCD X-ray Detector System from Mar-USA®. XRD patterns were obtained at 2 °C intervals (5 s exposures, 7 s dead time). The thermal cycle was 10–80 °C and back to 10 °C for PEO, and 10–150 °C for the copolymers.

Table 1
PE-*g*-PEO sample description

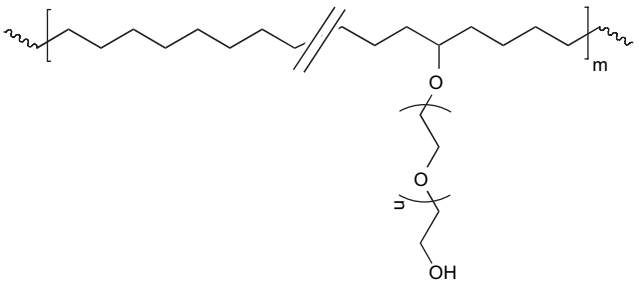

	PE-*g*-PEO**1**	PE-*g*-PEO**2**	PE-*g*-PEO**3**
Overall Mol. wt.	24,000	24,600	48,800
Polydispersity index – PE	2.02	2.26	2.77
Number of graft points per chain	9.6	7	8
n	25	50	100
PEO Mol. wt.	1200	2200	4400
Polydispersity index – PEO	1.1	1.08	1.08
Volume fraction of PEO (~373 K)	38	55	71
χN at 300 K (~ambient)	23	31	47
χN at 400 K (~PE molten)	12	16	25

One PEO graft per 100 CH_2 units; prepared by hydrogenation of polycyclooctene-*g*-PEO ($m \sim 150$) with 8 mol% PEGylated cyclooctene and 92% cyclooctene.

3.1. Analysis

The peaks from 1D WAXD profiles were analyzed in Matlab by piecewise least-squares profile fitting of the profiles in three q ranges ($q = 4\pi \sin\theta/\lambda$, 2θ is the scattering angle): low q (1.3–1.45 Å^{-1}), medium q (1.45–1.6 Å^{-1}) and high q (1.6–1.75 Å^{-1}). The peaks were modeled as Gaussians. A straight line was fitted to five points at each end of the segment and used as the baseline.

SAXS profiles were analyzed as described in our earlier papers [17,18]. In this model the scattering is resolved into two components: a central diffuse scattering due to independent scatterers that could be represented by:

$$I_D(q) = [a_1(\sin(a_2 q)/(a_2 q))]^2 \quad (1)$$

and by a broad interference peak at ~0.05 Å^{-1}. The interference peak is modeled as a product of an interface function due to a 1D lattice that is represented by a Gaussian and a shape factor that is modeled, as in Eq. (1), by a $\sin x/x$ function. The interference scattering is then written as:

$$I_L(q) = [(\sin(a_3 q)/(a_3 q))\{\mathrm{Gauss}(a_4, a_5, a_6)\}]^2/q^2 \quad (2)$$

where

$$\mathrm{Gauss}(a_4, a_5, a_6) = a_4 \exp\left[-0.5((q - a_5)/a_6)^2\right] \quad (3)$$

The intensities were calculated by numerical integration of the $I_D + I_L$ over the fitted region. This model is known to reproduce the observed scattering curve very well [17–19]. The *d*-spacing calculated from the position of the Gaussian peak in Eq. (3) is smaller than that calculated from the peak maximum in the raw data for two reasons: curve fitting uses Lorentz corrected data, and direct measurements of the peak position ignore the shift in the position of the peak that occurs when the interference function is multiplied by the shape function. This shift is insignificant when the lattice is large (sharp reflection), but the effect is pronounced when the lattice is quite small (broad reflections), about three or four unit cells bordering on being amorphous.

4. Results and discussion

4.1. Melting and recrystallization

Fig. 1 shows DSC scans of the three PE-*g*-PEO copolymers, and the results are summarized in Table 2. The melting point (T_m) of PEO is not visible in PE-*g*-PEO**1** and increases from 48 °C in PE-*g*-PEO**2** to 56 °C in PE-*g*-PEO**3**. This is consistent with the reported increase in T_m with the number of EO units (Fig. 2). This increase in T_m is accompanied by an increase in the crystallization temperature upon cooling (T_{cc}). PEO appears not to crystallize in PE-*g*-PEO**1**, and the T_{cc} increases from 18 °C in PE-*g*-PEO**2** to 28 °C in PE-*g*-PEO**3**. The T_m and T_{cc} of PEO in PE-*g*-PEO**2** are compared with those obtained by Inomata et al. [20] on poly(methyl acrylate)-*g*-PEO in Table 3; all PEOs have about the same molecular weight. As noted by Inomata

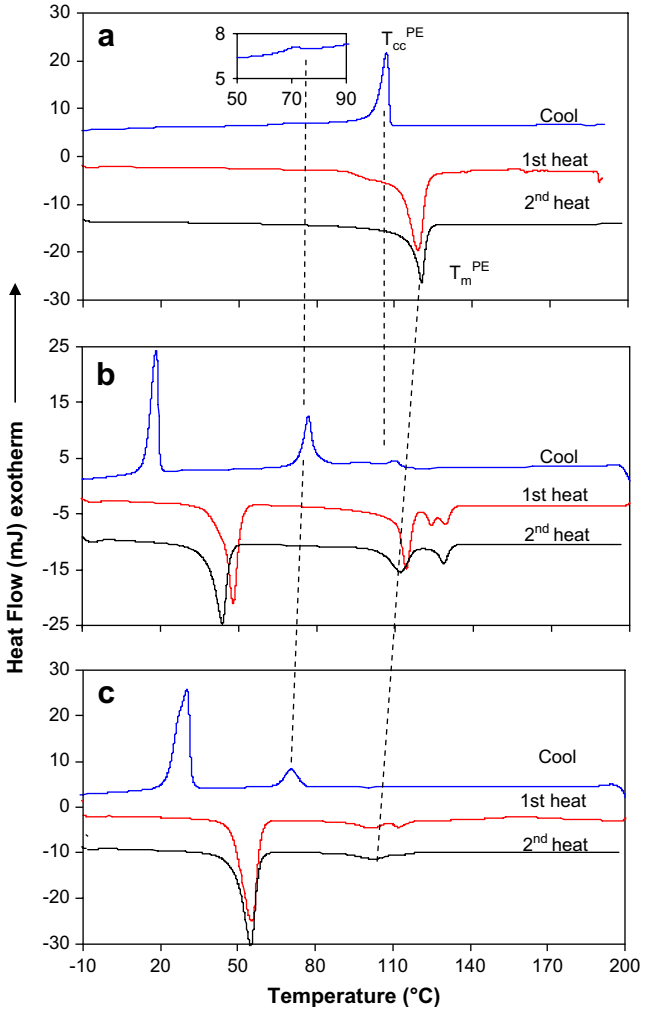

Fig. 1. DSC data for (a) PE-*g*-PEO**1**; (b) PE-*g*-PEO**2** and (c) PE-*g*-PEO**3**. The cool and reheat scans have been offset for clarity by the following amounts: (a) 5 and −12 mJ; (b) 0 and −7 mJ; and (c) 2 and −7 mJ. The vertical dashed lines show the changes in the crystallization and melting temperatures of PE with increase in length of PEO graft. The inset shows the 70 °C crystallization peak in PE-*g*-PEO**1**.

et al., the table shows that T_m (~50 °C) is not much affected by the main chain, but T_{cc} is considerably reduced, by as much as 16 °C in PE-*g*-PEO**2**. This indicates that the main chain impedes the crystallization but not the melting of the side chain. Note also that PMAC, which is amorphous, has a greater effect than PE, which is crystalline.

The grafted PEO also affect the melting and crystallization behavior of PE: the main T_m of PE decreases from 120 °C in PE-*g*-PEO**1**, to 115 °C in PE-*g*-PEO**2** and to 103 °C in PE-*g*-PEO**3**. The main T_{cc} is 106 °C in PE-*g*-PEO**1** and is most likely because PE chains are little affected by PEO at this particular composition. This T_{cc}

Table 2
Summary of DSC data in the form of melting temperatures (T_m) during heating and crystallization temperatures during cooling (T_{cc})

	T_m – first heat (°C)		T_{cc} – Cool (°C)			T_m – Reheat (°C)	
	PEO	PE	PEO	PE		PEO	PE
PE-*g*-PEO**1**	–	100^{s} and 120	–	106	~70^{vw}	–	120
PE-*g*-PEO**2**	48	115–130	18	108^{w} and 94^{w}	76	44	113–130
PE-*g*-PEO**3**	56	103–115	28	–	69	56	104–130

s – Shoulder; w – weak; vw – very weak.

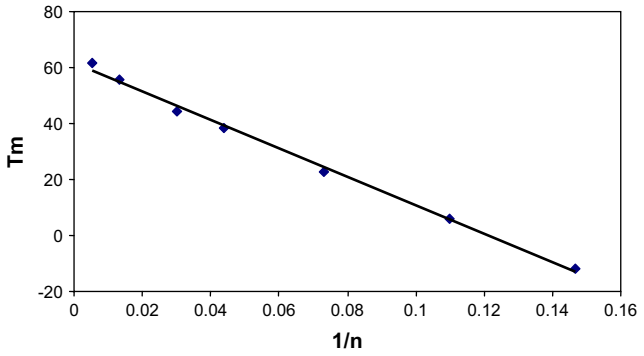

Fig. 2. Melting temperature of PEO as a function of the reciprocal of number of EO units (compiled from data sheets for Carbowax from Dow Inc.).

becomes weaker in PE-*g*-PEO**2** and disappears in PE-*g*-PEO**3**. A new lower T_{cc} appears in PE-*g*-PEO**2** at 76 °C, and further decreases to 69 °C in PE-*g*-PEO**3**. This lower T_{cc} peak, probably caused by PEO grafts that impede the crystallization of PE, is weak in PE-*g*-PEO**1** (at ~70 °C; inset in Fig. 1) and grows stronger with the increase in the graft length. The multiple endotherms at ~110 °C are attributed to the fractional crystallization of PE in the presence of the PEO grafts (see Section 4.3) [24].

4.2. Crystalline domains of PE and PEO

WAXD profiles of the three graft copolymers obtained at various temperatures during the heating cycle of the DSC scan are overlaid in Fig. 3 (profiles during cooling are not shown for clarity). Also shown for comparison is the profile from PEO homopolymer (Fig. 3a). The crystalline peaks in PE-*g*-PEO**1** (Fig. 3b) at 1.53 $Å^{-1}$ and 1.69 $Å^{-1}$ are the same as the 110 and 200 reflections, respectively, as in a PE homopolymer. The copolymers PE-*g*-PEO**2** and -PEO**3** (Fig. 3c and d) show crystalline peaks at 1.36 $Å^{-1}$ and 1.65 $Å^{-1}$, which are the same as the 120 and 032 reflections, respectively, as in PEO homopolymer [21]. Also profiles in these profiles are the 1.53 $Å^{-1}$ peak of PE, and the 1.65 $Å^{-1}$ peak is now a composite of both PEO and PE reflections.

As PEO is heated, it melts at ~50 °C and the crystalline peaks are replaced by an amorphous halo (Fig. 3a). Upon cooling, the PEO crystalline peaks appear at 40 °C. In PE-*g*-PEO**1**, the PE crystalline peaks disappear at 120 °C during heating (Fig. 3b) and reappear at 105 °C upon cooling. In PE-*g*-PEO**2** and PE-*g*-PEO**3**, three families of profiles can be identified, those due to PE and PEO up to 40 °C, those due to PE between 40 and 120 °C, and the amorphous scattering above 120 °C (Fig. 3c and d). In profiles obtained during cooling (not shown in the figure), PE peaks reappear as the polymer crystallizes at ~110 °C and PEO peaks appear between 20 and 30 °C. These data show that the main chain and the side chains crystallize into separate PE and PEO domains, respectively.

XRD patterns from solvent-cast films (7.5 mg/mL xylene solution at 100 °C and 50 min; cast on quartz or silicon substrates;

Table 3
Comparison of the melting and crystallization behavior of PEO in three graft copolymers with that of the homopolymer

Polymer	T_m (°C)	T_{cc} (°C)
PEO_{2000}	54	34
PE-*g*-61 wt% PEO_{2200}	48 (44 reheat)	18
PMAC[a]-*g*-57 wt% PEO_{2000}	48	−25
PMAC[a]-*g*-64 wt% PEO_{2000}	50	−6

[a] PMAC: poly(methyl acrylate) [20].

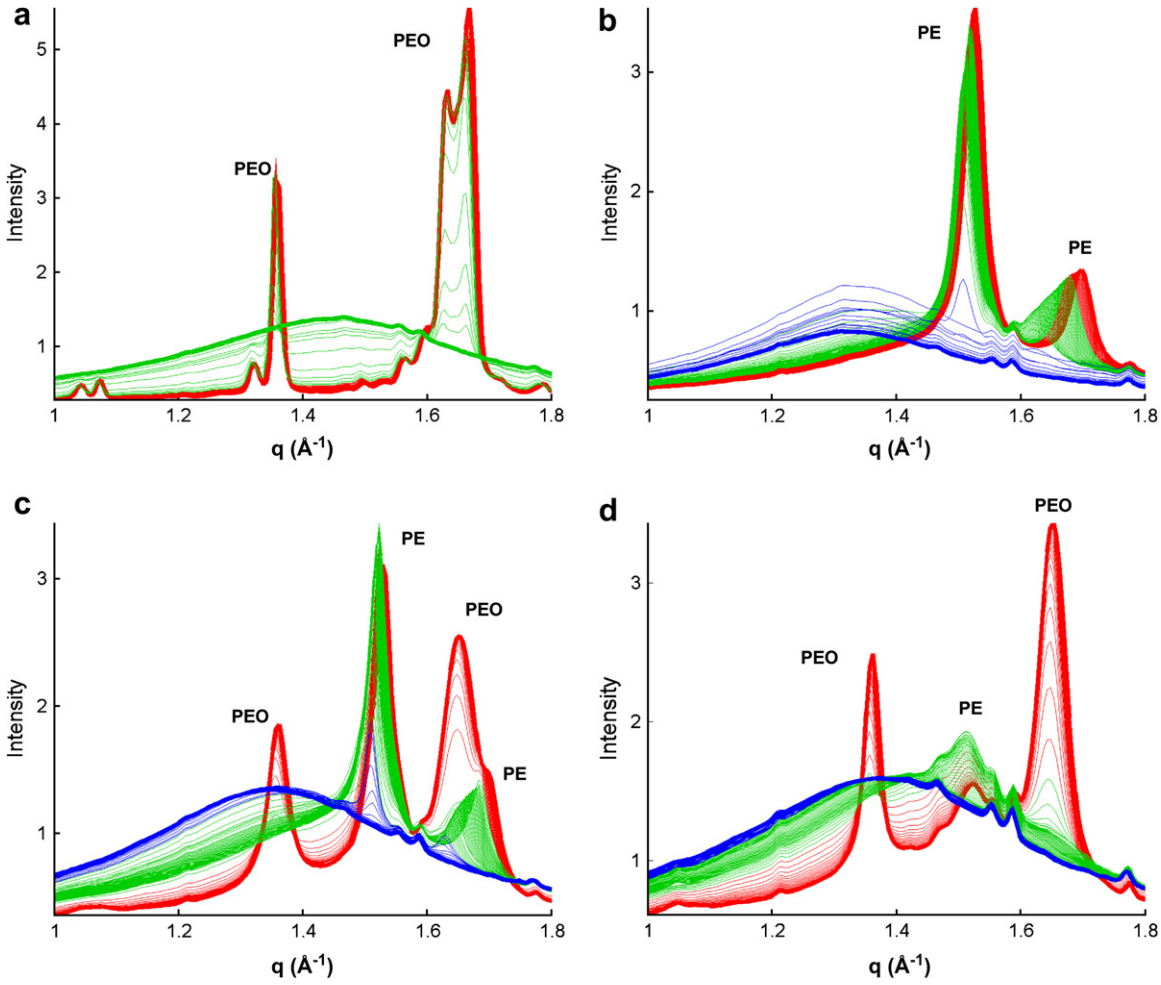

Fig. 3. Composite of WAXD profiles during in-situ DSC measurement: (a) PEO; (b) PE-*g*-PEO**1**; (c) PE-*g*-PEO**2**; (d) PE-*g*-PEO**3**. In these figures, we have attempted to color code the PEO^c–PE^c phase in red, PEO^m–PE^c in green and PEO^m–PE^m in blue; superscripts c and m refer to the crystalline and melt phase, respectively. The weak sharp peaks or wiggles at a few *q* values seen in all the traces are due to scattering from the DSC cell as verified with data obtained from samples in quartz capillaries. (For interpretation of the references to color in this figure legend, the reader is referred to the web version of this article.)

thickness ~0.1 mm) of the various graft copolymers were similar to that from the powders except that the amorphous halos were more intense. The PEO peaks were not observed in PE-*g*-PEO**1**. The two PEO peaks were weak in PE-*g*-PEO**2**, disappeared upon wetting and reappeared upon drying. The PEO domains could be swollen in water or ethanol without altering the mechanical integrity of the film. 2D XRD pattern of a stretched film did not show any orientation. This is consistent with the observed low elongation to break in these rather waxy films that tended to tear easily because of the low molecular weight of PE.

Thermal expansion of the PEO and PE unit cells was monitored using the peaks at $q = 1.36$ and $1.65\ Å^{-1}$ for PEO, and at $q = 1.53$ and $1.69\ Å^{-1}$ for PE. In PEO, as the temperature was increased from 10 to 80 °C, the shift in the $1.65\ Å^{-1}$ peak was much smaller than in the $1.36\ Å^{-1}$ peak (0.20 and $0.75\ Å^{-1}$, respectively) corresponding to greater expansion along the *a*-axis than along the *b*-axis (chain-axis is *c*). The increases in the *d*-spacings of 110 and 200 reflections of PE in the graft copolymers correspond to the expected thermal expansion of the PE unit cell with temperature up to about 50 °C and are in agreement with the unit-cell expansions for PE published by Tashiro [22] (Fig. 4). His empirical relations, obtained from data all the way into the melt, are plotted with a constant offset of between −0.005 and 0.02 Å to fit our data. While the effect of confinement by the PE lamellae on the thermal expansion of PEO crystals did not appear to be significant, there are significant deviations in the expansion characteristics of PE crystals above 50 °C, after the melting of PEO crystals, especially in the *b*-axis dimension. Thus, although the ambient PE lattice in the copolymer is similar to that of the homopolymer PE, indicating that PEO is not incorporated as a defect into the PE lattice, the differences in the changes with temperature suggest that grafted chains have significant effect on the crystallization and melting behavior of PE. This might account for the systematic changes in T_m and T_{cc} seen in the DSC scans.

4.3. Thermal fractionation and PE chain heterogeneity

The grafted chains interrupt the crystallizable sequences of PE, about every 100 carbons on the average. If the grafts were randomly placed one would expect a single broad endotherm. However, multiple melting peaks in the DSC scans suggest that the grafts may not be random.

There were changes in the SAXS and WAXD patterns accompanying these pre-melting transitions. A small jump was seen in the SAXS intensity vs. temperature plot of PE-*g*-PEO**2** at ~120 °C (data not shown). Fig. 5 shows the changes in the PE intensities in the WAXD of PE-*g*-PEO**2** in the temperature range of the multiple endotherms. As the polymer goes through the main melting peak, the intensity of the 110 reflection decreases by half, the peak

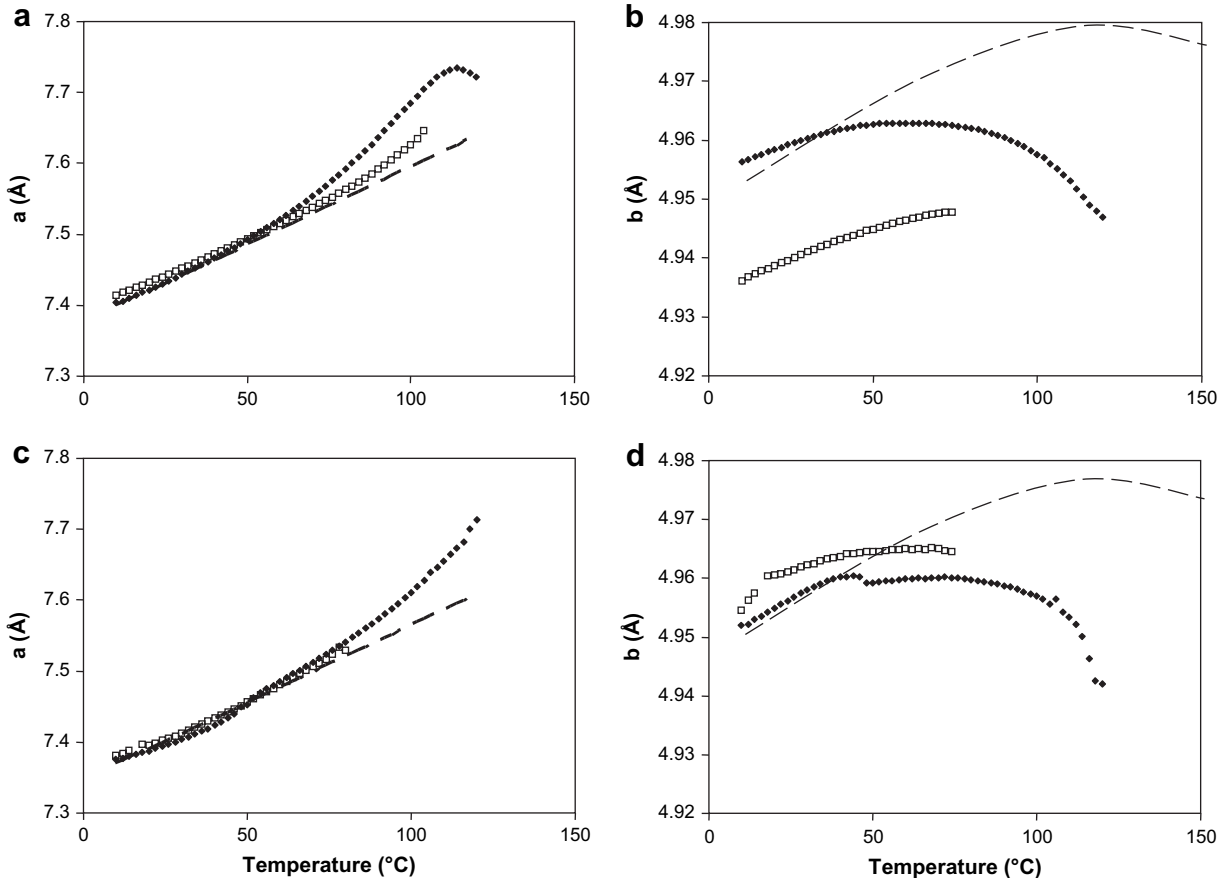

Fig. 4. Changes in the unit-cell dimensions of the PE lattice in the copolymer: (a and b) PE-*g*-PEO**1**; (c and d) PE-*g*-PEO**2**. Left panel (a and c) shows the *a*-axis and the right panel (b and d) the *b*-axis. Filled and open symbols refer to the heating and cooling parts of the cycle, respectively. Dotted lines are Tashiro's data [22].

becomes sharper and the 200 reflection abruptly shifts to a lower *q* value. These profiles show that PE remains crystalline in the orthorhombic phase until it completely melts at 134 °C. Since reorganization would lead to a new phase, hexagonal phase for instance [23], the continuation of the orthorhombic phase suggests that the multiple endotherm is not due to melting and reorganization of the PE chains in the crystalline phase but due to fractionation [24].

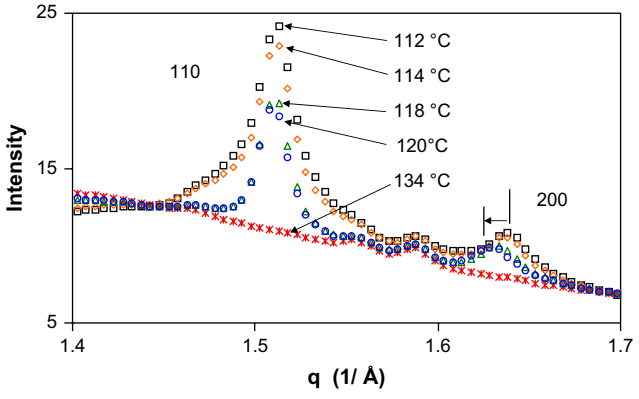

Fig. 5. Overlay of the WAXD profiles in PE-*g*-PEO**2** at temperatures spanning the multiple endothermic transitions showing the changes in the PE intensity. The profiles at 112 and 114 °C (squares and diamonds, respectively) are prior to main melting peak. The profiles at 118 and 120 °C (triangles and circles, respectively) are just after the main melting peak but before the weaker melting peaks (see Fig. 1). The profile at 134 °C without a peak (asterisks) is past the complete melting event. The peak at q = 1.59 A^{-1} is from the sample holder and is present in all the scans.

4.4. Small-angle scattering and correlation with DSC and WAXD data

The SAXS profiles obtained during heating in a DSC cell are shown in Fig. 6 for the PEO homopolymer and the three graft copolymers. These were obtained from as-polymerized powders. Data were also obtained from melt- and solution-cast films, and there were no significant differences among these different types of samples. The profiles in Fig. 6 were selected from several complete sets of data; plots for PEO and PE-*g*-PEO**3** are from the second heating cycle, and those for the PE-*g*-PEO**1** and PE-*g*-PEO**2** are from the first heating cycle. The differences between the profiles obtained during the first heat and the second heat were mostly in the relative heights of the various orders of the interference peaks in SAXS, in the width of the transitions and in the features of the doublet prior to complete melting in the DSC. But, the essential features of the transition discussed below were the same.

The SAXS peaks in the PEO sample (Fig. 6a) are due to PEO lamellae, and showed the expected behavior upon heating and cooling. The peaks remained unchanged during the initial stages of heating, began to shift to smaller angles as the lamellar-spacing increased from 153 Å to ~160 Å, and finally disappeared at 50 °C. The crystalline peaks in the WAXD patterns began to decrease at 50 °C, disappeared at 60 °C, and thus existed even in the absence of long-range structure. The process was reversed upon cooling; the WAXD peaks appeared at 42 °C before the appearance of SAXS peak, and reached a plateau at 32 °C; the SAXS peaks appeared at 34 °C and shifted to larger angles as the sample was cooled further and the *d*-spacing decreased from 168 Å to 162 Å. Thus, short-range order appears to be a pre-requisite for the lamellar order, both

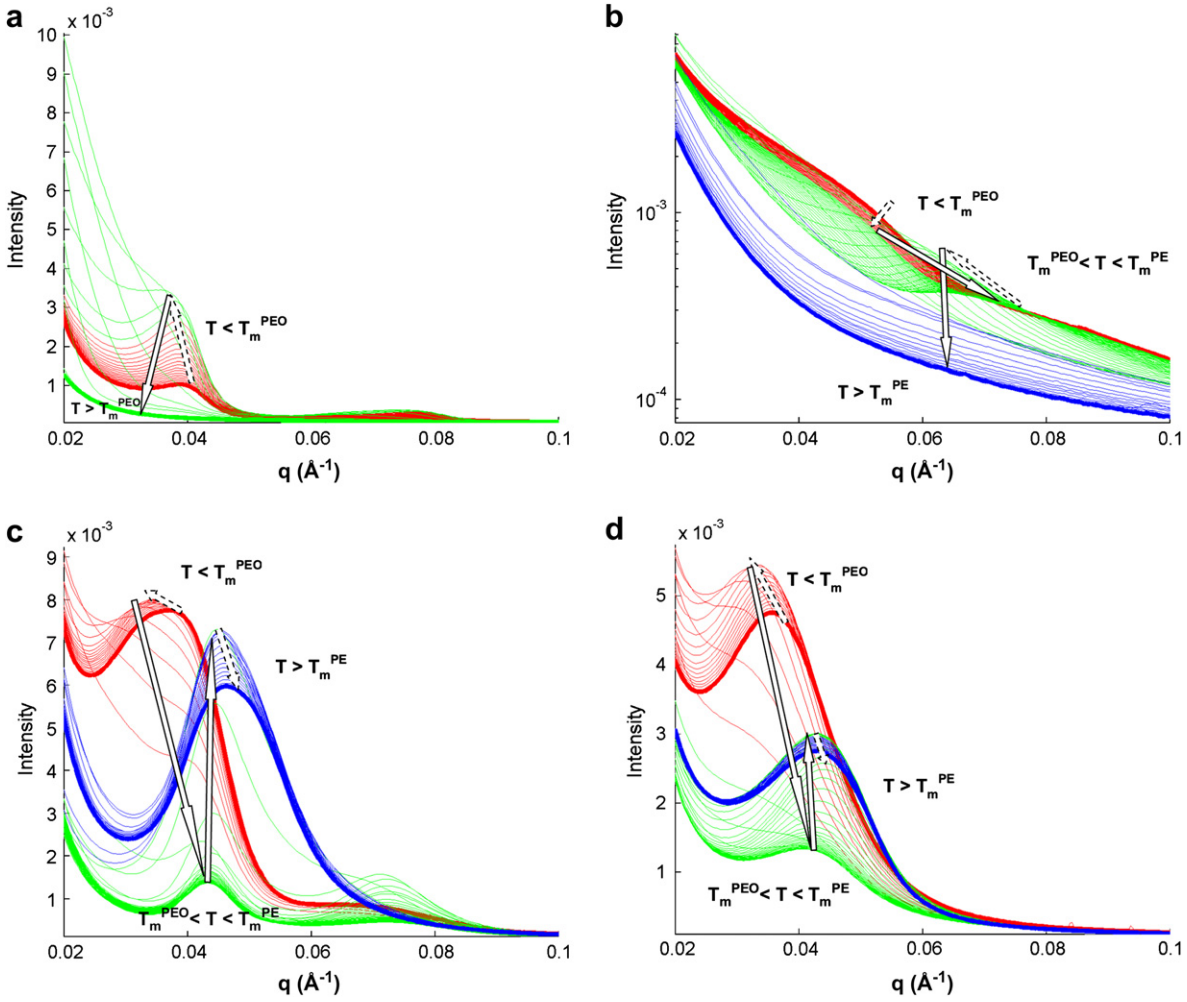

Fig. 6. Overlay of time-resolved SAXS profiles obtained with a time resolution of 12 s (5 s exposure and 7 s dead time) while the samples are heated at 10 °C/min. The figure shows intensity (relative scale) versus scattering vector (q) at various temperatures (T): (a) PEO; (b) PE-*g*-PEO**1**; (c) PE-*g*-PEO**2**; (d) PE-*g*-PEO**3**. In these figures, PEO^c–PE^c phase in shown in red, PEO^m–PE^c in green and PEO^m–PE^m in blue; superscripts c and m refer to the crystalline and melt phase, respectively. Note that the intensity in b is on a logarithmic scale. Gradual changes in pattern are indicated by dotted arrows, and abrupt changes are marked by solid arrows. (For interpretation of the references to color in this figure legend, the reader is referred to the web version of this article.)

during heating and cooling. This is in contrast to the "SAXS before WAXD" observations on other polymers such as poly(butylene terephthalate) and polypropylene [25–27].

The SAXS peaks in PE-*g*-PEO**1** (Fig. 6b), which can be discerned only when the profiles are plotted on a logarithmic scale, are too weak for meaningful interpretation. However, following observations can be made based on the similarities of this profile to those of other two copolymers (see next paragraph). As the sample is heated, the spacing of the SAXS peak first increases from ~120 Å, and a new, relatively intense peak with a *d*-spacing ~90 Å appears at 70 °C. The spacing then increases to >100 Å, and the peak finally disappears as the polymer melts at 120 °C. Upon cooling, a peak appears at ~105 °C as PE crystallizes, its *d*-spacing decreases from ~180 to ~150 Å, and the peak nearly disappears as the polymer is cooled to ambient temperature.

The features in the SAXS profiles from PE-*g*-PEO**2** and PE-*g*-PEO**3** (Fig. 6c and d) were similar to each other and are summarized in Table 4. Relevant parameters are plotted as a function of temperature in Fig. 7 for PE-*g*-PEO**3**. Both the crystalline and the SAXS peaks track the melting endotherm during heating and the crystallization exotherm during cooling. The *d*-spacing of the SAXS peak, which we attribute to lamellae, increases slightly at the beginning of the heating cycle. Melting of PEO crystals at ~50 °C results in a large decrease in the lamellar-spacing and peak

Table 4
Summary of SAXS data in Fig. 7 for two of the copolymers across the various transition points. Superscripts "c" and "m" refer to the crystalline and molten states, respectively. The temperatures are deduced from the SAXS scans

Regimes	I	Transition temperatures	II	Transition temperatures	III
Phases	PE^c–PEO^c		PE^c–PEO^m		PE^m–PEO^m
Heating segment	*d*-spacings (Å)	PEO melting (°C)	*d*-spacings (Å)	PE melting (°C)	*d*-spacings (Å)
PE-*g*-PEO**2**	166–170	45	144	118	134
PE-*g*-PEO**3**	136–148	50	125	108	127
Cooling segment		PEO-crystallizing (°C)		PE crystallizing (°C)	
PE-*g*-PEO**2**	148	12	132–140	78	134
PE-*g*-PEO**3**	136	22	122–125	73	127

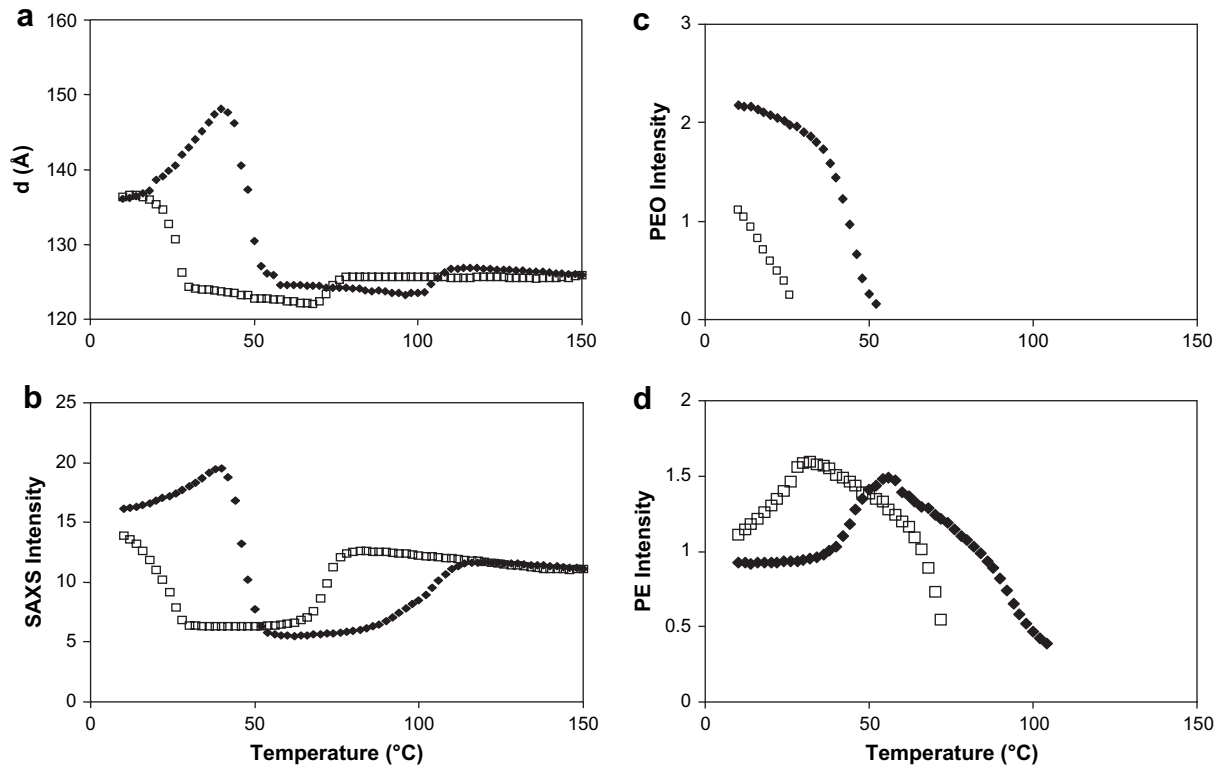

Fig. 7. Changes in the structural parameters with temperature in PE-*g*-PEO**3** as seen in: (a) the SAXS *d*-spacings; (b) the intensity of the first SAXS peak; (c) the intensity of the PEO reflection (WAXD) at 1.36 $Å^{-1}$, and (d) the intensity of the PE reflection (WAXD) at 1.53 $Å^{-1}$. These plots were derived from the profiles in Fig. 6d. Filled symbols correspond to heating segment and the open symbols to the cooling segment.

intensity. Surprisingly, as the temperature is increased to ~110 °C and PE crystals melt as evidenced by the disappearance of the crystalline peaks in the WAXD, there is a large increase in the spacing and the intensity and of the SAXS peak. The SAXS peak remains essentially unchanged up to 150 °C, the highest temperature for these profiles. The process is reversed upon cooling, although not along the same path seen during heating because of the obvious differences between melting and crystallization temperatures; the transformation shows hysteresis. SAXS peaks seen in melt changes over to lamellar peak upon the crystallization of PE at ~70 °C. This peak remains unchanged until the onset of PEO crystallization at ~25 °C. As during heating, crystallization of PE and PEO, is accompanied by sudden changes in the *d*-spacing and the intensity of the lamellar peak.

4.5. Interpretation of SAXS patterns

The large changes in both the SAXS peak intensity and the *d*-spacings with temperature (Figs. 6 and 7) clearly suggest that large-scale reorganization accompany melting of PEO at ~50 °C and the melting of PE at ~115 °C. The changes in the SAXS peak intensities across three distinct temperature regimes (Table 4) can be qualitatively interpreted in terms of the changes in the electron density contrast between the domains made of PEO segments and the PE chains [28,29] (Fig. 8). The SAXS peak in regime I ($T_m^{PE} > T > T_m^{PEO}$) is clearly due to PE lamellae. The peak at $T > T_m^{PE}$ could be attributed to microphase separated structures with either hydrophilic PEO-rich molten droplets in a molten hydrophobic PE-rich matrix, or vice versa depending on the relative volume fraction. In the solid phase at $T < T_m^{PEO}$, given that WAXD shows crystalline peaks of both PE and PEO, one could argue that there are two separate domains of PE and PEO lamellae, or that one polymer chain is inserted into the crystals of another. Since the two chains are not miscible, the similarity between the WAXD profiles of PE before and after the melting of PEO, the observation of a single, albeit broad SAXS peak as well as previously published data on PE–PEO diblock copolymers [11], suggest that a lamellar structure with alternating layers of PE and PEO crystals is most likely.

The SAXS intensity in the pre-T_m^{PEO} regime can be attributed to the 0.059 e/$Å^3$ difference in the electron density between crystalline PE (PE^c, 0.344 e/$Å^3$) and crystalline PEO (PEO^c, 0.403 e/$Å^3$ (Fig. 8a)). Given that the electron density of molten PEO (PEO^m) is 0.352 e/$Å^3$, the large decrease in SAXS intensity that occurs when PEO melts at ~50 °C is explained by the large decrease in the electron density difference from 0.059 (PE^c–PEO^c) to 0.008 e/$Å^3$ (PE^c–PEO^m) (Fig. 8b). The decrease in the *d*-spacing could be because melting of the PEO grafts relaxes the constraints on the folding of the PE chains, causing the PE chains to snap into a new lamellar phase, accompanied perhaps by an increase in PE

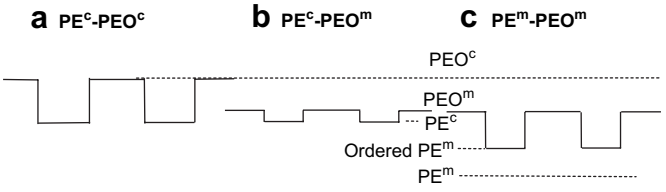

Fig. 8. Interpretation of the changes in the SAXS intensities with temperatures in terms of the changes in electron density profiles (vertical axis shows the electron density and the horizontal axis corresponds to distances in the microphase separated domains): (a) pre-T_m^{PEO} in which both PE and PEO are crystalline; (b) after the melting of PEO but before the melting of PE, $T_m^{PEO} < T < T_m^{PE}$, in which lamellae are due to PE; (c) post-T_m^{PE} in which both PE and PEO segments are molten. The electron densities of the crystalline and molten PE and crystalline and molten PEO are represented by PE^c (0.344), PE^m (0.248), PEO^c (0.403) and PEO^m (0.352), respectively. The values in parenthesis are the values of electron density in electron per $Å^3$.

crystallinity. This assertion is supported by the WAXD patterns (Fig. 7d): there is a large increase in the PE intensity as PEO melts during heating and corresponding decrease in the PE intensity as PEO crystallizes during cooling.

In the regime $T_m^{PEO} < T < T_m^{PE}$, SAXS spacing and the intensity remains essentially unchanged until PE melts at ~115 °C. Since the electron density of molten PE (PE^m) is 0.248 e/Å^3, the increase in SAXS peak intensity when both PE and PEO are molten can be attributed to the increase in the contrast from 0.008 (PE^c–PEO^m) to 0.104 (PE^m–PEO^m) e/Å^3 (Fig. 8c). The intensity in the melt is lower than that expected from the electron densities of the molten PE and PEO perhaps because of the residual ordering of the PE chains that raises the electron density of the PE domains as indicated in the figure. The increase in the *d*-spacing could be attributed to the increased volume of the melt phase. SAXS peak in the melt, which is present after all the different populations of PE crystallites are molten at 130 °C, is one of the key observations in this study.

One feature in the SAXS *d*-spacings is that the *d*-spacing in every temperature regime is larger in PE-*g*-PEO**2** than in PE-*g*-PEO**3** even though the PEO block size in the latter is larger (50 vs. 100): 12–15 Å in the PE^c–PEO^c and PE^c–PEO^m phases and 7 Å in the melt. The most likely explanation is that the degree of interdigitation is different in the two polymers, being greater in the PE-*g*-PEO**3** polymer with larger number of EO blocks [11].

4.6. Phase separation in the solid and the melt phases

Both DSC and XRD data show that the main PE chains and the grafted PEO side chains crystallize into separate domains. Differences in the melting and crystallization temperatures of PE and PEO make this is an interesting system for studying confined crystallization of both PEO and PE. Such studies have been carried out with diblock copolymers, such as ethylene/styrene–ethylene–butene [30]; in this instance, PE crystallites are surrounded by an amorphous matrix, and the packing of the microdomains established by self-assembly in the melt was preserved during the crystallization of PE even though the matrix block was well above its T_g. In our PE-*g*-PEO copolymer, the microphase separated structures that are present in the melt transform into lamellar structures, the PE crystals coexist with PEO crystals, and the crystallization kinetics of one component is influenced by the presence by the other.

The phase state of block copolymers is usually discussed in terms of χN, where χ is the Flory–Huggins segment–segment interaction parameter and N is the degree of polymerization. In the case of PE-*g*-PEO, N is the sum of the average number of ethylene segments between PEO grafts and the number of monomers in one PEO grafts. χ at any temperature T can be calculated using the relation $\chi(\mathrm{E/EO}) = -0.2802 + 177.4/T$, obtained from the published work on PE-*b*-PEO diblock copolymers [15]. Although this relation is derived for block copolymers, one can get a sense of the strengths of the interaction between the segments in the graft copolymer. The calculated values of χN (Table 1) in all the polymers are greater than 10 at which order–disorder transition is predicted to occur in diblock copolymers (volume fraction 0.5) [1]. Thus, PE-*g*-PEO copolymer is expected to show phase segregated structures and give rise to a SAXS peak over the entire range of temperature used here. In PE-*g*-PEO**1** when $\chi N \sim 10$ at 400 K, the SAXS peak was not visible.

Block copolymers are known to exhibit complex but predictable phase behavior in the solid and melt phases [2,11,31–35]. For instance, in diblock copolymers of poly(oxyethylene) (PEO) and poly(oxybutylene), which have polar and non-polar moieties as in PE-*g*-PEO, disordered [31] or lamellar phase [32] found in the melt transform under shear and heat into a gyroid phase [32], all of which give characteristic SAXS peaks. In one of the few published work on graft copolymers, Inomata et al. found that while crystallization of PEO in PMMA-*g*-PEO leads to the microphase separation in the solid phase, homogeneous miscibility of the PEO and PMMA segments at higher temperatures can account for the absence of any SAXS peak in the melt [20]. In copolymers of PE and PEO, where the interaction parameter between the hydrophobic PE and the hydrophilic PEO is unfavorable for mixing even in the melt, there is an even greater tendency towards lamellar microphase separation in the solid state in these copolymers as seen in our work on graft copolymers, and in the work of Zhu and coworkers on block copolymers [11,15]. However, there are differences between the scattering profiles in the melt of diblock and graft copolymers. SAXS peaks observed in diblock PE–PEO copolymers were attributed to correlation holes [11,15] because of the smaller length of PE and PEO blocks (29 E and 20 EO repeat units, respectively) that result in smaller value of χN (~ 10). In contrast, no SAXS peaks were observed in our PE-*g*-PEO copolymers when the PEO chain length was ~25, and the peaks observed at PEO chain lengths of 50 and 100 are clearly due to microphase separation. Furthermore, while our SAXS patterns showed dramatic changes in SAXS intensity across the phase boundaries, those from PE–PEO diblock copolymers did not show any such behavior during melting of PE either at slow heating that resulted in disordered melt accompanied by correlation hole scattering or at fast heating that resulted in an ordered melt.

5. Conclusions

SAXS peaks were observed in both the solid and the melt phases for a polymer consisting of a hydrophobic PE backbone and hydrophilic PEO graft. These peaks are due to microphase separation. The formation of separate PEO and PE domains in the solid state is accompanied by crystallization. In the melt, amphiphilic nature of PE-*g*-PEO graft copolymers give rise to PEO-rich molten droplets in a molten PE-rich matrix, or vice versa depending on the relative volume fraction. The small-angle X-ray scattering profiles change dramatically with temperature as PE-*g*-PEO copolymers pass through three different phases: both polymers solid ($T < T_m^{PEO}$), one polymer molten ($T_m^{PEO} < T < T_m^{PE}$) and both polymers molten ($T > T_m^{PE}$). These changes correspond to the differences in the microphase structures in the three temperature regimes, which could be different from that in block copolymers. The crystalline domains of the PE main chain and the PEO side chains are similar to those in the corresponding homopolymers, and there is clear evidence of fractionation of PE crystals due to the heterogeneity in the graft-spacings. PE chains decrease the onset of crystallization of PEO blocks from 34 to18 °C. The PEO grafts affect the crystallization behavior of PE main chain as seen in the decrease in the major melting event from 120 to 103 °C, and the decrease in the temperature of crystallization during cooling from 106 to 69 °C.

Acknowledgements

We thank Mr. Wenjie Wang for his assistance with synchrotron measurements, Mr. Herman Minor for preliminary DSC data and Profs. Manfred Stamm and David Grubb for discussions on the interpretation of the data and for reviewing the paper. The work at the University of Vermont was supported by an EPA grant X-83239001-0 to the New England Green Chemistry Consortium (NEGCC). The work at Rutgers University was supported by an NSF grant (DMR-0735242), and that the University of Massachusetts was supported by the grant NSF-CTS 0553957 and facilities support of the Materials Research Science and Engineering Center at UMass., Amherst. Portions of this work were performed at the DuPont–Northwestern–Dow Collaborative Access Team (DND-CAT) Synchrotron Research Center located at Sector 5 of the Advanced Photon Source. DND-CAT is supported by the E.I. DuPont de

Nemours and Co., The Dow Chemical Company, the U.S. National Science Foundation through Grant DMR-9304725 and the State of Illinois through the Department of Commerce and the Board of Higher Education Grant IBHE HECA NWU 96. Use of the Advanced Photon Source was supported by the U.S. Department of Energy, Office of Science, Office of Basic Energy Sciences, under Contract No. W-31-109-ENG-38.

References

[1] Leibler L. Macromolecules 1980;13:1602–17.
[2] Bates FS, Schulz MF, Khandpur AK, Förster S, Rosedale JH, Almdal K, et al. Faraday Discuss 1994;98:7–18.
[3] Hadjichristidis N, Pispas S, Floudas GA. Block copolymers: synthetic strategies, physical properties and applications. Chichester, UK: John Wiley and Sons, Ltd,; 2002.
[4] Abetz V, Simon PFW. Phase behaviour and morphologies of block copolymers. In: Abetz V, editor. Advances in polymer science – block copolymers I, vol. 189. Springer; 2005. p. 125–212.
[5] Hamley IW. The physics of block copolymers: Oxford University Press; 1999.
[6] Hamley IW. Developments in block copolymer science and technology. Wiley; 2004.
[7] Muller AJ, Balsamo V, Arnal ML. Nucleation and crystallization in diblock and triblock copolymers. In: Abetz V, editor. Advances in polymer science – block copolymers II, vol. 190. Berlin, Heidelberg: Springer; 2005. p. 1–63.
[8] Shuyan Q, Chakraborty AK, Wang H, A.Lefebvre A, Balsara NP, Shakhnovich EI, et al. Phys Rev Lett 1999;82:2896–9.
[9] Eitouni HB, Rappl TJ, Gomez ED, Balsara NP, Qi S, Chakraborty AK, et al. Macromolecules 2004;37:8487–90.
[10] Kreig A, Lefebvre AA, Hahn H, Balsara N, Qi S, Chakraborty AK, et al. J Chem Phys 2001;115:6243–51.
[11] Sun L, Liu Y, Zhu L, Hsiao BS, Avila-Orta CA. Polymer 2004;45:8181–93.
[12] Nojima S, Kiji T, Ohguma Y. Macromolecules 2007;40(21):7566–72.
[13] Hamley IW, Castelletto V, Castillo RV, Mueller AJ, Martin CM, Pollet E, et al. Macromolecules 2005;38(2):463–72.
[14] Breitenkamp K, Simeone J, Jin E, Emrick T. Macromolecules 2002;35: 9249–52.
[15] Sun L, Liu Y, Zhu L, Hsiao BS, Avila-Orta CA. Macromol Rapid Commun 2004; 25:853–7.
[16] Hammersley AP, Svensson SO, Thompson A, Graafsma H, Kvick Å, Moy JP. Rev Sci Instrum [SRI-94] 1995;66:2729–33.
[17] Murthy NS, Akkapeddi MK, Orts WJ. Macromolecules 1998;31:142–52.
[18] Murthy NS, Wang Z-G, Hsiao BS. Macromolecules 1999;32:5504–99.
[19] Wang Z-G, Hsiao BS, Murthy NS. J Appl Crystallogr 2000;33:690–4.
[20] Inomata K, Nakanishi E, Sakane Y, Koike M, Nose T. J Polym Sci Part B Polym Phys 2005;43:79–86.
[21] Takahashi Y, Hiroyuki T. Macromolecules 1973;6(5):672–5.
[22] Tashiro K. Comp Theoret Polym Sci 2001;11:357–74.
[23] Murthy NS, Correale ST, Kavesh S. Polym Commun 1990;31:50–2.
[24] Muller AJ, Arnal ML. Prog Polym Sci 2005;30:559–603.
[25] Alison HG, Davey RJ, Garside J, Quayle MJ, Tiddy GJT, Clarke DT, et al. Phys Chem Chem Phys 2003;5:4998–5000.
[26] Hsiao BS, Wang Z-G, Yeh F, Gao Y, Sheth KC. Polymer 1999;40:3515–23.
[27] Wang Z-G, Hsiao BS, Sirota EB, Agarwal P, Srinivas S. Macromolecules 2000; 33:978–89.
[28] Todokoro H. Structure of crystalline polymers. New York: Wiley; 1979.
[29] Rigby D, Sun H, Eichinger BE. Polym Int 1997;44:311–30.
[30] Loo Y-L, Register RA, Ryan AJ. Phys Rev Lett 2000:84.
[31] Mai S-M, Fairclough JPA, Terrill NJ, Turner SC, Hamley IW, Matsen MW, et al. Macromolecules 1998;31:8110–6.
[32] Hamley IW, Fairclough JPA, Ryan AJ, Mai SM, Booth C. Phys Chem Chem Phys 1999;1:2097–101.
[33] Matsen MW, Bates FS. J Chem Phys 1997;106:2436–48.
[34] Bates FS, Fredrickson GH. Phys Today 1999;(2):32–8.
[35] Bates FS, Fredrickson GH. Ann Rev Phys Chem 1990;41:525–57.